I&EC research
Industrial & Engineering Chemistry Research

Article

pubs.acs.org/IECR

PhotoATRP-Based Fluorinated Thermosensitive Block Copolymer for Controllable Water/Oil Separation

Yin-Ning Zhou, Jin-Jin Li, and Zheng-Hong Luo*

Department of Chemical Engineering, School of Chemistry and Chemical Engineering, Shanghai Jiao Tong University, Shanghai 200240, P. R. China

Supporting Information

ABSTRACT: The increasing environmental burden in human society calls for the development of more environmentally benign technologies and sustainable applications. Wastewater contaminated by oil or organic solvents has become a serious environmental issue nowadays. Herein, a well-defined thermosensitive block copolymer was designed and used for controllable water/oil separation. The functional material poly(2,2,3,4,4,4-hexafluorobutyl methacrylate)-*block*-poly(*N*-isopropylacrylamide) was synthesized through a new environmentally benign "living" radical polymerization technique [i.e., photoinitiated atom-transfer radical polymerization (photoATRP)]. The synthesized functional copolymer was considered as a modifier for fabricating a smart surface with thermal-responsive wettability. The switchable mechanism, surface composition, and morphology of the as-fabricated surface were investigated by water contact-angle measurement, X-ray photoelectron spectroscopy, and atomic force microscopy. Results showed that the as-fabricated surface can reversibly switch between the hydrophilicity and hydrophobicity, which results from the synergistic effect of surface chemical composition, reorientation of the functional groups, and roughness in response to the temperature. On the basis of mechanism understanding, a smart separation device was constructed and used for separating water/oil mixtures. The separation of a water/hexane layered mixture has high penetration fluxes of 2.50 L s^{-1} m^{-2} for water and 2.78 L s^{-1} m^{-2} for hexane, while exhibiting a good efficiency of over 98%.

1. INTRODUCTION

Functional polymers for surface modifications have gained increasing attention in the past few years.[1−4] Compared to traditional monofunctional polymers, fluorinated polymers have remarkable and unique bulk properties, including excellent chemical resistance, thermostability, and low refractive index.[5,6] By using a fluoropolymer-based coating, surfaces with hydrophobicity, low adhesive, low friction coefficients, and antifouling behaviors can be achieved because of the low surface energy of fluoroalkyl.[7−14] For example, Yu and Luo fabricated a superhydrophobic and low-adhesive surface with a water contact angle (WCA) of 161° and contact-angle hysteresis of less than 5° using fluorosilcone polymer-grafted silica hybrid nanoparticles.[7] van Zoelen et al. prepared fluorinated amphiphilic polymer coatings with effective antifouling properties against the algae *Ulva linza* and *Navicula diatoms*.[14]

In addition to conventional polymer coatings, the increasing demands on smart surfaces with tunable wettability further boost great interest in the development of high-performance functional polymers.[15,16] Such materials can be applied in various fields, including a controlled-release platform,[17−20] water/oil separation,[21−27] and so on. The external stimuli used nowadays for controlling the surface wettability involves the pH,[28−31] electric potential,[32−34] light,[35−38] and temperature.[39−45] Among them, a thermal-responsive strategy is thought to be a facile and safe approach for industrial application, especially in on-demand and environmentally friendly applications. Poly(*N*-isopropylacrylamide) (PNIPAAm) with a lower critical solution temperature (LCST) of 32 °C is considered to be a thermosensitive polymer with an industrial application perspective.[46] To our knowledge, the wettability of the surfaces modified by surface-grafted PNIPAAm or coated by PNIPAAm hydrogel can be regulated by adjusting the temperature.[47,48] However, the improvement of flat-surface wettability through homopolymer modification is limited to some extent. In order to overcome the problems, block copolymers are often employed to provide polymeric materials with comprehensive functionality. For example, Xue et al. fabricated a smart surface with tunable oil/water wettability by using thermosensitive poly(methyl methacrylate)-*b*-poly(*N*-isopropylacrylamide) (PMMA-*b*-PNIPAAm), in which the hydrophobic PMMA acts as a physical cross-link of the hydrophilic PNIPAAm.[43]

Atom-transfer radical polymerization (ATRP) was known as a brilliant tool for preparing polymers with well-defined structures (e.g., block, brush and star copolymer) and is also efficient for fluoromonomers.[49,50] Unfortunately, utilization of a stoichiometric low-oxidation-state transition-metal catalyst causes the time-consuming oxygen and catalyst removal process in a traditional ATRP system. Considerable work has been devoted to diminishing the catalyst dosage of the ATRP technique.[51−54] More recently, photoinitiated ATRP (photoATRP) joins in the ATRP family as a new "low catalyst" member and paves the way for temporal-controllably synthesizing well-defined polymers under environmentally benign conditions (e.g., without heating, low catalyst dosage).[55−60]

Received: July 2, 2015
Revised: September 14, 2015
Accepted: October 13, 2015

DOI: 10.1021/acs.iecr.5b02394
Ind. Eng. Chem. Res. XXXX, XXX, XXX−XXX

Scheme 1. Synthetic Route of the Fluorinated Block Copolymer via PhotoATRP

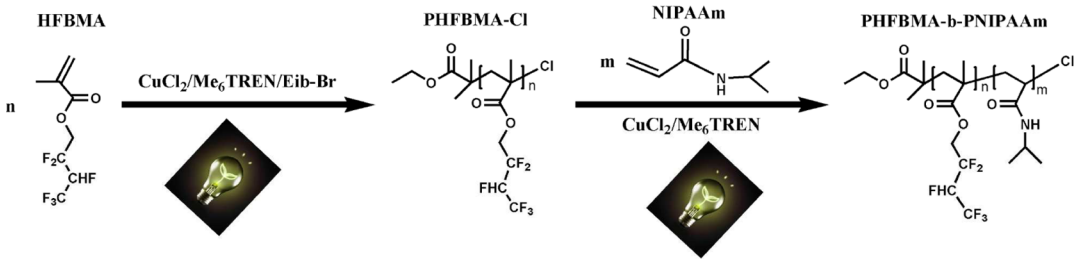

For example, Haddleton and Matyjaszewski demonstrated the detailed investigations on the mechanism of photoATRP that act as a guide for the synthesis of well-defined polymers in high yields.[58−60]

In this work, a well-defined thermal-responsive block copolymer, poly(2,2,3,4,4,4-hexafluorobutyl methacrylate)-*block*-poly(*N*-isopropylacrylamide) (PHFBMA-*b*-PNIPAAm), was synthesized through sequential photoATRP, as shown in Scheme 1. The synthesized functional copolymer was utilized for the fabrication of a smart surface with thermal-responsive wettability. The switchable thermal-responsive wettability, surface composition, and morphology of the as-fabricated surface were investigated. Furthermore, as a proof-of-concept, the resulting copolymer solution was directly cast onto a stainless steel mesh for temperature-controlled water/oil mixtures separation. The resultant mesh acted as a "water-removing" separation unit below the LCST of PNIPAAm and as an "oil-removing" device above the LCST. The novelty of this work lies in the new thermal-responsive block copolymer that was prepared through a newly developed and environmentally friendly ATRP technique (photoATRP), as well as its use for the fabrication of a smart surface that provides a sustainable application in controllable water/oil separation.

2. EXPERIMENTAL SECTION

2.1. Materials. 2,2,3,4,4,4-Hexafluorobutyl methacrylate (HFBMA; 96%, Xeogia Fluorine−Silicon Chemical Co. Ltd., China) was rinsed with an aqueous NaOH (5 wt %) solution to remove inhibitor before use. *N*-Isopropylacrylamide (NIPAAm; 97%, TCI (Shanghai) Development Co., Ltd.) was recrystallized from a toluene/hexane solution (1:2, v/v) and dried under vacuum before use. Ethyl 2-bromoisobutyrate (Eib-Br; 98%, Adamas), hexamethylated tris(2-aminoethyl)amine (Me_6TREN; 99%, Alfa Aesar), and $CuCl_2$ (99%, Acros) were used as received. The stainless steel meshes with 350 mesh size were cleaned by ethanol and acetone rinsing prior to use.

2.2. Synthesis of Macroinitiator PHFBMA-Cl. To a Schlenk flask with a magnetic stirrer were added $CuCl_2$ (0.43 mg, 3.2×10^{-3} mmol), HFBMA (3.0 mL, 16 mmol), and *N*,*N*-dimethylformamide (DMF)/cyclohexanone (1:1, v/v; 3.0 mL). The flask was sealed by a rubber stopper and subjected to three freeze−pump−thaw cycles. Subsequently, Me_6TREN (4.9 μL, 1.9×10^{-2} mmol) was added under nitrogen. The mixture was stirred for 5 min until the homogeneous complex was obtained, and then it was subjected to three additional freeze−pump−thaw cycles. Finally, the reaction flask was put into a photochemical reactor after Eib-Br (23.5 μL, 0.16 mmol) was added to the mixture by using a syringe. The reaction was stopped by immersing the flask into liquid nitrogen before exposure to air at a predetermined conversion. Then, it was diluted with chloroform and passed through a neutral alumina column to remove the copper complex. The resulting polymer was precipitated from a 3 M hydrochloric acid (HCl)/methanol solution. The polymer was purified through repeated dissolution and precipitation (three times) and dried under vacuum. At time intervals, samples were taken by syringe for kinetic analysis (yield, 3.05 g; conversion, 75.9%).

2.3. Synthesis of Block Copolymer PHFBMA-*b*-PNIPAAm. The block copolymer was synthesized using PHFBMA-Cl as the macroinitiator. First, PHFBMA-Cl (750 mg, 4.0×10^{-2} mmol), $CuCl_2$ (0.54 mg, 4.0×10^{-3} mmol), and DMF/cyclohexanone (1:1, v/v; 2.0 mL) were added to a Schlenk flask with a magnetic stirrer. The flask was sealed by a rubber stopper, and the mixture was stirred for a while until the macroinitiator dissolved. Then, a solution of NIPAAm (905 mg, 8.0 mmol) and 3 mL of DMF/cyclohexanone were added to the flask, followed by three freeze−pump−thaw cycles. Subsequently, Me_6TREN (6.2 μL, 2.4×10^{-2} mmol) was added under nitrogen. The mixture was stirred for 5 min until the homogeneous complex was obtained, and then it was subjected to three additional freeze−pump−thaw cycles. Finally, the reaction flask was put into a photochemical reactor to start polymerization. The reaction was stopped by immersing the flask into liquid nitrogen before exposure to air at a predetermined conversion. It was diluted with chloroform and passed through a neutral alumina column to remove the copper complex. The resulting polymer was precipitated from *n*-hexane. The block copolymer was purified through repeated dissolution and precipitation (three times) and dried under vacuum. At time intervals, samples were taken by syringe for kinetic analysis (yield, 1.43 g; conversion, 75.1%).

2.4. Reactor. The photochemical reactor consisted of a high-pressure mercury lamp equipped with a UV filter ranging from 300 to 400 nm ($\lambda_{max} \sim 365$ nm) and a circulating-water cooling system. The reaction environmental temperature was 40 °C, and the intensity of the light source was 15 ± 0.5 mW cm^{-2}.

2.5. Preparation of Copolymer Films. The silicon wafers were successively cleaned in a beaker using a 10% HCl and KF solution, acetone, ethyl alcohol, and deionized water in an ultrasonic bath. Then, silicon wafers were dried by a nitrogen stream before use. The polymer solution (5 wt % in THF) was spin-coated onto the cleaned smooth silicon wafers at 3000 rpm for 30 s. These samples were used for WCA measurement, atomic force microscopy (AFM) measurement, and X-ray photoelectron spectroscopy (XPS) measurement. The block-copolymer-coated stainless steel mesh was obtained by a polymer solution (5 wt % in THF) casting drop by drop. All of the as-prepared samples were dried naturally at ambient temperature for 12 h (most of the solvent was evaporated slowly) and under vacuum at 60 °C for another 24 h.

2.6. Measurements. *2.6.1. Nuclear Magnetic Resonance (NMR).* Monomer conversion was determined by ^{1}H NMR spectroscopy on a 400 MHz Varian Mercury plus 400 in $CDCl_3$ with a tetramethylsilane internal standard.

2.6.2. Gel Permeation Chromatography (GPC). The molar mass (M_n) and dispersity (M_w/M_n) of the polymer were analyzed on a GPC (Tosoh Corp.) equipped with two HLC-8320 columns (TSK gel Super AWM-H, pore size = 9 μm; 6 × 150 mm, Tosoh Corp.) and a refractive index detector (Bryce) consisting of a double-path, double-flow system at 30 °C. The elution phase was DMF (0.01 mol L^{-1} LiBr, elution rate = 0.6 mL min^{-1}), and a series of poly(methyl methacrylate) (PMMA) were used as the conventional calibration standard.

2.6.3. Differential Scanning Calorimtery (DSC). Thermal analysis of the polymers was carried out using a differential scanning calorimeter (TA Instruments Q2000) under a dry nitrogen atmosphere. Dry nitrogen was purged into the DSC cell at a flow rate of 50 mL min^{-1}. The samples were first heated at a rate of 10 °C

DOI: 10.1021/acs.iecr.5b02394
Ind. Eng. Chem. Res. XXXX, XXX, XXX−XXX

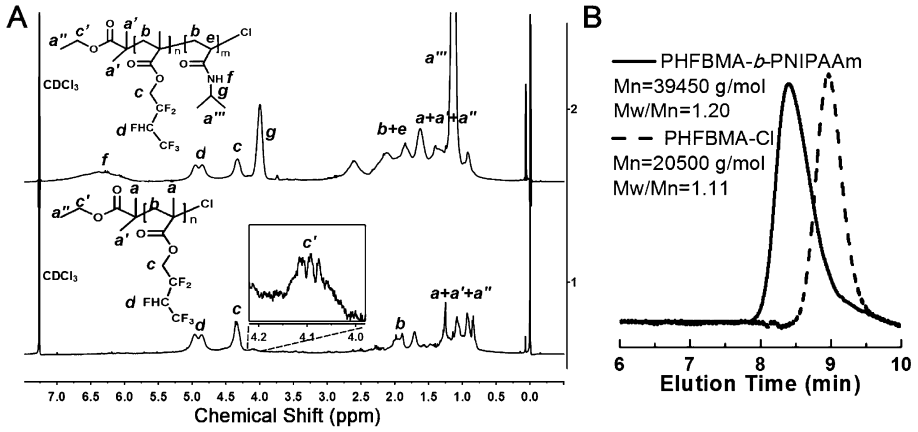

Figure 1. (A) ^{1}H NMR spectra of PHFBMA-Cl (bottom) and PHFBMA-*b*-PNIPAAm (top). (B) GPC traces of PHFBMA-Cl (right) and PHFBMA-*b*-PNIPAAm (left).

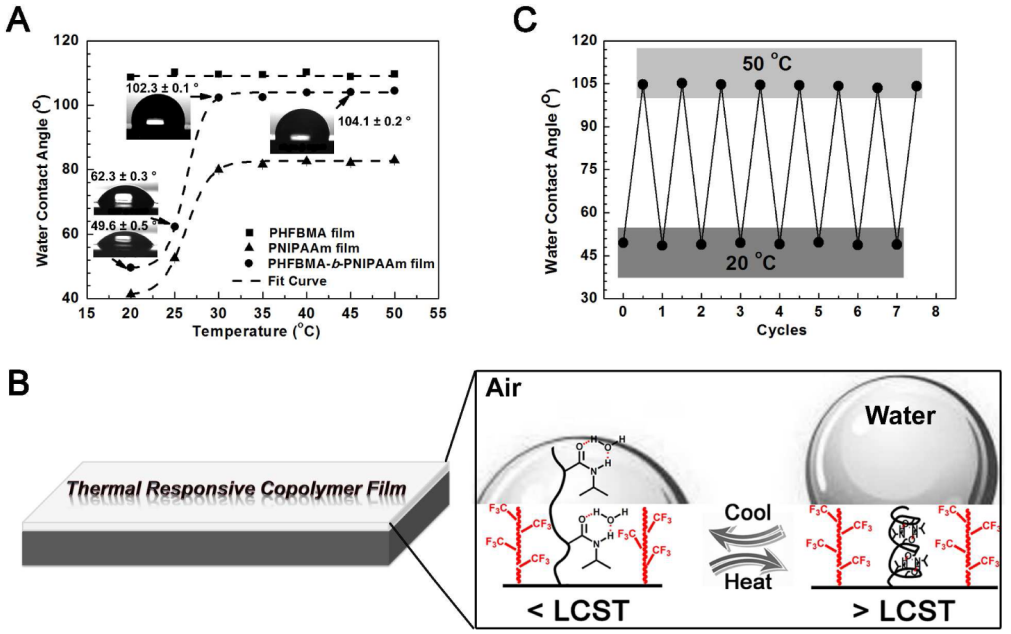

Figure 2. (A) Temperature dependences of WCA for the various modified surfaces. The WCAs were maintained at about 109° for the PHFBMA film, changed from 41° to 83° for the PNIPAAm film, and changed from 50° to 104° for the PHFBMA-*b*-PNIPAAm film with the temperature increasing from 20 to 50 °C (the insets are representative WCA images). (B) Schematic representation of the intermolecular (<LCST) and intramolecular (>LCST) hydrogen-bonding interaction for the transformation of hydrophilicity and hydrophobicity. (C) Reversible WCA transition of the block copolymer film at 20 °C (<LCST) and 50 °C (>LCST).

min^{-1} to 200 °C and held at 200 °C for 3 min to eliminate thermal history. The samples were then cooled to −20 °C before being reheated to 200 °C at a rate of 10 °C min^{-1}. All data associated with the glass transition measurements were obtained from the second heating scan and taken as the midpoint of the heat capacity change.

2.6.4. Contact Angle (CA) Measurement. The static water or oil CA of a silicon surface functionalized by a block copolymer was measured on a Contact Angle Measuring Instrument (KRUSS, DSA30) at temperatures of 20, 25, 30, 35, 40, 45, and 50 °C using the sessile drop method. The temperature was controlled by a TC40-MK2 temperature controller. A deionized water droplet (3 μL) was dropped onto the samples, which were kept at the required temperature for 10 min.

2.6.5. AFM. The surface morphology and roughness of spin-coated films were acquired on an AFM instrument using a Dimension Icon scanning probe microscope equipped with a Nanoscope V controller (Bruker) in the tapping mode at room temperature in air. A RTESPAW-300 silicon cantilever (Bruker) with a pyramid tip of radius 8 nm was used. The set-point amplitude was 80.61 mV. The scan rate and number of scan lines were 0.999 Hz and 256, respectively.

2.6.6. XPS. XPS spectra were acquired through a Kratos Axis Ultra DLD spectrometer (Kratos Analytical A Shimadzu Group Company) using a monochromatic Al Kα X-ray beam as the excitation source (1486.6 eV). The analyzer used hybrid magnification mode (both electrostatic and magnetic), and the takeoff angle was 90°. Measurements of the samples in dry and wet states were carried out according to the previous work.[61] Before measurement of the samples in the wet state, the spin-coated samples were wetted by water droplets for 2 h and dried under vacuum for another 2 h. After that, the samples were immediately measured. The dried ones were measured directly after sample preparation without further treatment.

2.6.7. Scanning Electron Microscopy (SEM). The morphologies of the samples were observed by field-emission scanning electron microscopy (FE-SEM; JEOL JSM-7401F). The samples were treated by platinum sputtering.

DOI: 10.1021/acs.iecr.5b02394
Ind. Eng. Chem. Res. XXXX, XXX, XXX−XXX

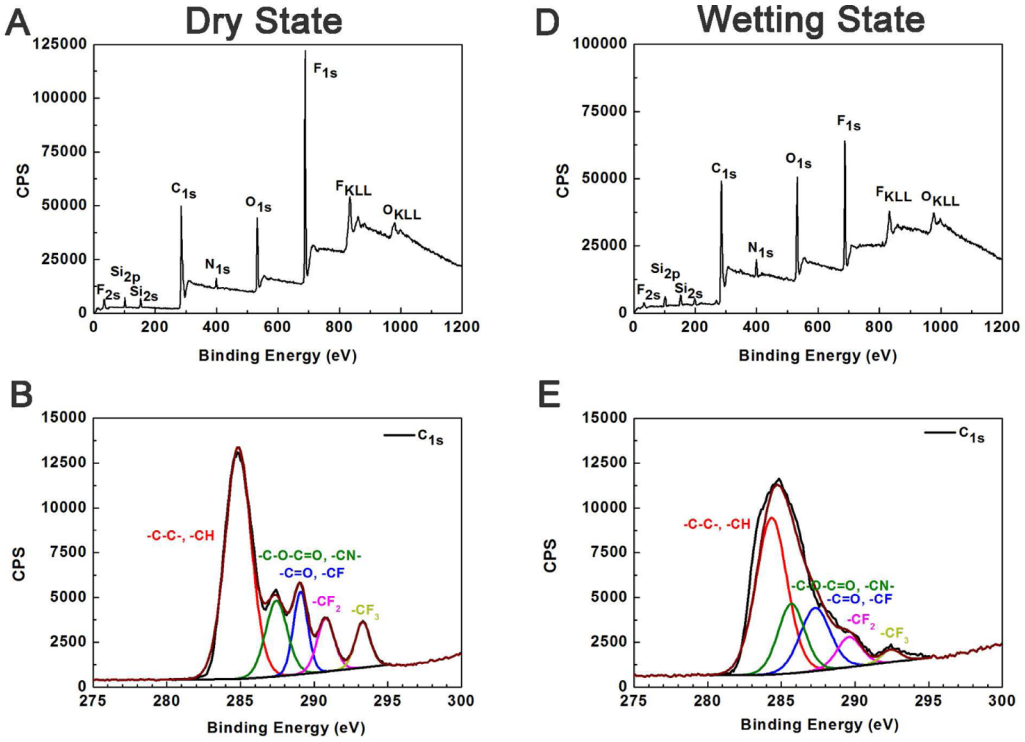

C

Surface Composition (%)				Bulk Composition (%)	
C_{1s}	N_{1s}	O_{1s}	F_{1s}	N	F
56.11	2.38	14.35	27.16	7.14	23.92

F

Surface Composition (%)				Bulk Composition (%)	
C_{1s}	N_{1s}	O_{1s}	F_{1s}	N	F
63.29	4.40	17.41	14.90	7.14	23.92

Figure 3. XPS spectra results of the as-fabricated surface decorated by the PHFBMA-*b*-PNIPAAm film: (A) survey scan spectrum; (B) high-resolution C_{1s} spectrum; (C) quantification of C_{1s}, N_{1s}, O_{1s}, and F_{1s} recorded at the dry state; (D) survey scan spectrum, (E) high-resolution C_{1s} spectrum; (F) quantification of C_{1s}, N_{1s}, O_{1s}, and F_{1s} recorded at the wetting state.

3. RESULTS AND DISCUSSION

3.1. Synthesis of PHFBMA-Cl and PHFBMA-*b*-PNIPAAm by PhotoATRP. PhotoATRP of HFBMA was initially carried out on the basis of optimized polymerization conditions.[62] As one of the merits of photoATRP, a high-oxidation-state catalytic complex [copper(II) salt] was chosen as the catalyst, and the amount of the catalyst was at the parts per million (ppm) level with respect to the monomer.

Figure 1A shows the ^{1}H NMR spectra of the resulting polymers. In spectrum 1 at the bottom, the characteristic peaks at 4.8−5.0 and 4.1−4.2 ppm (depicted in the enlarged view) are assigned to the proton of −CHF− and the methylene protons of the initiator ($-OCH_2CH_3$), respectively. On the basis of the ^{1}H NMR results, the degree of polymerization (DP_n) of PHFBMA is 75, namely, M_n(NMR) is 18800 g mol^{-1}. The M_n and M_w/M_n of PHFBMA-Cl obtained by GPC (Figure 1B) is 20500 g mol^{-1} and 1.11, respectively. Subsequently, the chain extension of the PHFBMA-Cl macroinitiator was successfully performed using a second monomer (NIPAAm) under polymerization conditions, which can be confirmed through spectrum 2 at the top of Figure 1A and the GPC curve in Figure 1B. The characteristic signs at 4.0 and 6.0−7.0 ppm correspond to the methine proton of the isopropyl group and the amide proton next to the isopropyl group, respectively. By calculating the peak area of PNIPAAm at 4.0 ppm and that of PHFBMA at 4.8−5.0 ppm, DP_n of PNIPAAm is 150. Therefore, the resulting block copolymer is denoted as $PHFBMA_{75}$-*b*-$PNIPAAm_{150}$, and M_n(NMR) is 35700 g mol^{-1}. In addition, as observed from Figure 1B, the GPC trace of $PHFBMA_{75}$-*b*-$PNIPAAm_{150}$ moves toward the high-molar-mass direction, M_n is 39450 g mol^{-1}, and M_w/M_n is 1.20. These results imply that the end fidelity of the first block prepared by photoATRP is high. The kinetics study shown in Figure S1 demonstrates that both reactions follow pseudo-first-order kinetics after a short induction period and show a typical feature of living polymerization. In particular, the robust temporal control protocol in photoATRP was also investigated and supported through a kinetic plot, as depicted in Figure S1.

3.2. Switchable Wettability of As-Fabricated Surfaces. It is well-known that the PNIPAAm-modified flat surface can undergo a temperature-induced wettability transition from hydrophilicity to hydrophobicity.[47] However, the hydrophilic PNIPAAm homopolymer will become amorphous upon exposure to an aqueous environment, which is unsuitable for practical application. Therefore, a fluorinated polymer segment was introduced in this work, which not only improves the hydrophobicity of the resulting copolymer-modified surface but also can be considered as an effective supporting framework for PNIPAAm.

As shown in Figure 2A, the wettability of the modified surface with fluorinated homopolymer is independent of the temperature. The WCA remains at about 109.0° in the whole temperature range. In contrast, the wetting property of the surface modified by the PNIPAAm film or fluorinated block copolymer film is sensitive to the temperature. Compared to

DOI: 10.1021/acs.iecr.5b02394
Ind. Eng. Chem. Res. XXXX, XXX, XXX−XXX

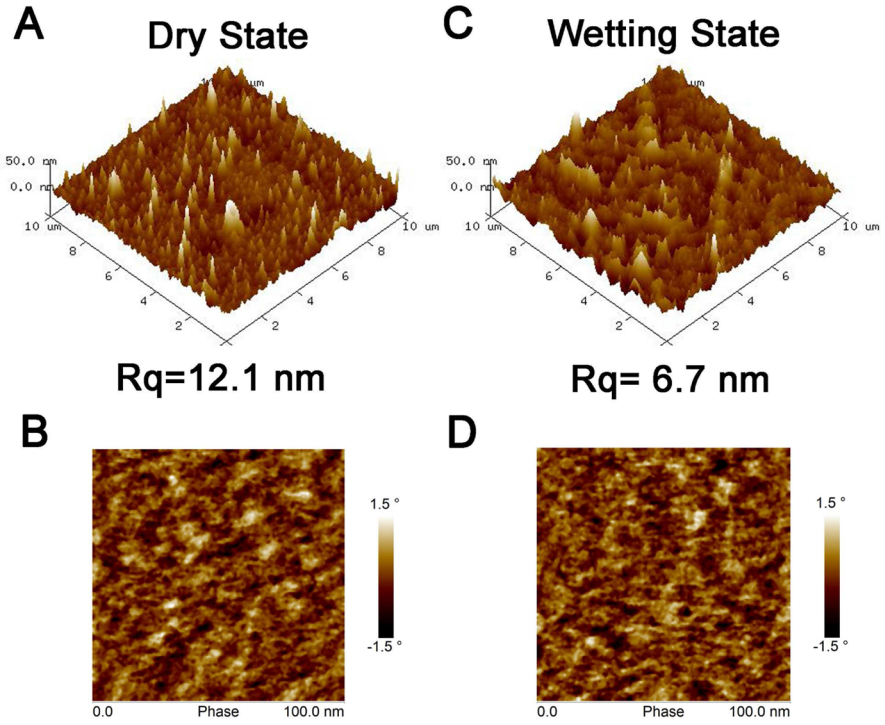

Figure 4. AFM images of the as-fabricated surface decorated by the PHFBMA-*b*-PNIPAAm film: (A) height and (B) phase images observed at the dry state; (C) height and (D) phase images observed at the wetting state.

the PNIPAAm film with limited responsive wettability, the PHFBMA-*b*-PNIPAAm film causes the wettability transition from hydrophilicity to hydrophobicity in response to the external temperature. One can find that the WCA first increases from 49.6° to 102.3° with an increase of the temperature from 20 to 30 °C, followed by a slight increase to 104.1° at 40 °C. It remains at the maximum value even at elevated temperatures from 40 to 50 °C. The thermal-responsive surface wettability can be explained by the formation of an intermolecular or intramolecular hydrogen bond involved in PNIPAAm chains below or above the LCST of about 32 °C. As schematically illustrated in Figure 2B, the predominate hydrogen bonding below the LCST is the intermolecular action between NIPAAm units and H_2O molecules, while intramolecular hydrogen bonds formed between the C═O and N−H groups in NIPAAm moieties at a temperature above LCST. The former effect can promote extension of the PNIPAAm chains, contributing to the hydrophilicity of an as-fabricated surface. The letter one causes collapse of the PNIPAAm chains, leading the surface to exhibit hydrophobicity.[47] In addition to the controllability of the surface wettability, its reversibility was also examined by recycling the temperature from 20 to 50 °C. After seven cycles, there is only a negligible attenuation of the wettability, which indicates that the thermal-responsive switch of this modified surface is stable (Figure 2C).

To further probe the wetting property, the surface composition and morphology were detected by XPS and AFM, respectively. Figure 3 presents the XPS spectra of the block copolymer film on a silicon wafer before and after wetting. In Figure 3A,D, the characteristic peaks located at 689, 531, 399, and 285 eV are attributed to F_{1s}, O_{1s}, N_{1s}, and C_{1s} core levels, respectively, which confirm that the surface was covered with the PHFBMA-*b*-PNIPAAm copolymer film. However, the relative intensity of F_{1s} in Figure 3D is lower than that in Figure 3A, which is likely due to surface reorganization of the copolymer chains. The content of fluorinated species (27.16%) on the surface before wetting is found to be higher than that in bulk (23.92%), as listed in Figure 3C. This phenomenon is usually considered to be the surface enrichment of fluorinated segments, which results from the low surface energy of fluorine.[8−13] However, after wetting the surface, the result in Figure 3F shows that the content of the fluorinated species decreases to 14.90% and becomes lower than the bulk content. Interestingly, we find that the content of nitrogen on the surface increases from 2.38% at the dry state to 4.40% at the wetting state. The change of the surface chemical composition confirms the reorganization of short perfluoroalkyl and acidamide groups. In addition, various carbon-based groups can be analyzed by resolving the complex pattern of the peak of the high-resolution C_{1s} spectra, as illustrated in Figure 3B,E. Specifically, five discrete Gaussian fitting peaks, including C−C/C−H at 284.8 eV, −C−O−C═O/−C−N− at 287.4 eV, −C═O/−CF at 289.0 eV, $-CF_2$ at 290.8 eV, and $-CF_3$ at 293.3 eV, are well observed and consistent with the chemical bonding environments of the synthesized copolymer. However, there is a dramatic difference of the C_{1s} peak pattern between the spectra, and the intensities of the $-CF_2$ and $-CF_3$ peaks decrease drastically after wetting the surface. The result is attributed to the synergistic effect of exposure of the acidamide groups and reorientation of the perfluoroalkyl groups.[61] These unique characteristics endow the as-fabricated functional surface with stable hydrophobicity at a temperature above LCST.

From the height image (Figure 4A) of the surface modified by the PHFBMA-*b*-PNIPAAm film at the dry state, the nanostructure with 12.1 nm of the root-mean-square roughness (R_q) can be seen within the 100 μm^2 region. In addition, the AFM phase image of the film at the dry state (Figure 4B) shows that the PHFBMA domains are separate from the PNIPAAm domains, which is confirmed by the separated bright and dark

DOI: 10.1021/acs.iecr.5b02394
Ind. Eng. Chem. Res. XXXX, XXX, XXX−XXX

domains. On the basis of thermal property analysis (Figure S2 in the Supporting Information), the PHFBMA block is softer than the PNIPAAm block, which is indicated by their different glass transition temperatures. Thus, the PHFBMA blocks appear brighter in the phase image. When the surface is wetted by a water droplet, R_q decreases to 6.7 nm, and the morphology becomes smoother than before, as shown in Figure 4C. Compared to the phase image at the dry state (Figure 4B), the PNIPAAm domains become more obvious and occupy more surface area at the wetting state, as shown in Figure 4D. These results indicate that the as-fabricated surface has a rough copolymer film with micro- and nanostructure, which can enhance the wetting behavior of substrates according to the theoretical model.[16]

Overall, as a result of the synergistic effect of the surface chemical composition, reorientation of the functional groups, and the roughness, reversibly regulating the wetting property of the as-fabricated surface between hydrophilicity and hydrophobicity was achieved at temperatures below and above LCST.

3.3. Application of Water/Oil Separation. Water/oil separation as an important environmental, economic, and social issue has received considerable attention.[25] In this field, different functional materials with special wettability (i.e., hydrophobicity, hydrophilicity, oleophobicity, and oleophilicity) can be used to fabricate water/oil separators. By the merit of the thermosensitive block copolymer, the controllable surface wettability inspires us to fabricate a water/oil separation unit.

Herein, a common industrial stainless steel mesh with 350 mesh size was functionalized by a simple method, namely, polymer solution casting, which shows great advantages of fast fabrication compared to other methods.[43] Figure 5A shows the SEM image of the noncoated stainless mesh, which is knitted by metal wires with an average diameter of about 35 μm. Also, the formed square-shaped pore size is 45 × 45 μm^2. As shown in Figure 5B, the mesh is covered with a homogeneous copolymer film without obvious defects through casting of a 2 mL polymer solution (5 wt % in THF) onto a round mesh with an area of 2.37×10^{-3} m^2. The knitted metal wires are still visible, and their average diameter increases to about 39 μm after solution casting. Moreover, the zoom-in image shows that the microstructure of the film is smooth.

Prior to the use of a coated mesh for water/oil separation, CA measurements were carried out to study the controllable wettability of the coated mesh regulated by the temperature. Generally, the typical surface tension of oils is 20−30 mN m^{-1}; therefore, the materials used directly for preparing the oleophobic surface are limited, which requires their surface energy to be lower than the surface tension of oils.[25] Without exception, the as-fabricated mesh decorated by the fluorinated block copolymer has oleophilicity that is independent of the external temperature and becomes superoleophilic with the help of an increase of the surface roughness. One can find that the oil droplet (*n*-hexane) spreads out as soon as it contacts with the mesh, as shown in Figure 5C. However, the water wettability of the mesh is found to be dependent on the temperature. The WCA on the coated mesh measured at 20 °C is 39.5°, and that is 129.8° at 50 °C, as illustrated in the left panels of Figure 5D,E. Compared to the results of the flat silicon wafer modified by a similar polymer film (Figure 2A), both the hydrophilicity and hydrophobicity are enhanced, owing to the increase of the surface roughness. This is important for the water/oil separation. Furthermore, besides the oil CA in air, underwater oil CA characterizations at different temperatures (the right panels of Figure 5D,E) show that the as-fabricated mesh is oleophobic under water. The difference between the underwater oil CAs is attributed to the different PNIAAm chain conformations, which leads to the different hydrophilicities. Importantly, the enhanced oleophobicity at below LCST can effectively avoid the oil permeating the mesh as the water flows through the prepared separation unit.

Owing to the switchable wettability, the as-prepared mesh is promisingly used in the field of water/oil separation. As a proof-of-concept, a controllable water/oil separation system was constructed, as demonstrated in Figure 6. The as-fabricated mesh (the effective filtration area is 0.96×10^{-3} m^2) was fixed between two glass apparatuses with flanged connection, and a

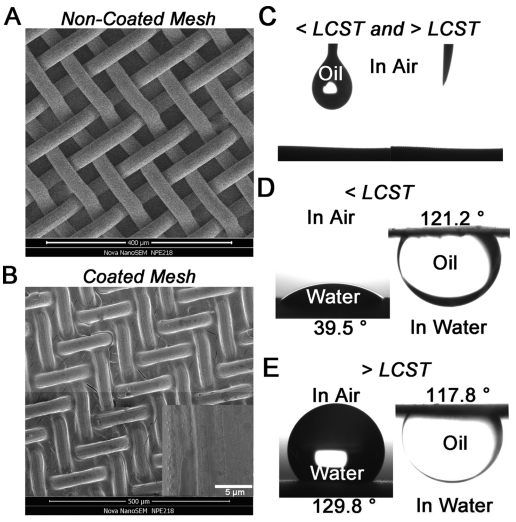

Figure 5. SEM and CA images of the stainless steel mesh: (A) noncoated mesh; (B) coated mesh; (C) oil CA on the coated mesh in air; (D) WCA and underwater oil CA on the coated mesh at 20 °C (<LCST); (E) WCA and underwater oil CA on the coated mesh at 50 °C (>LCST).

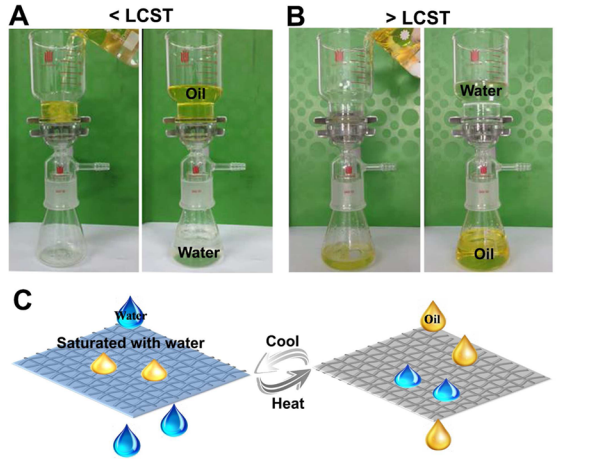

Figure 6. Thermal-responsive water/oil separation process: (A) water passes through the mesh, and oil (*n*-hexane dyed by ferrocene) stays at the upper glass container at below LCST; (B) oil penetrates through the mesh, and water remains at the upper glass container at above LCST. (C) Schematic illustration of the mechanism of separation.

DOI: 10.1021/acs.iecr.5b02394
Ind. Eng. Chem. Res. XXXX, XXX, XXX−XXX

conical flask was placed at the bottom as the liquid receiver. To ensure that separation proceeds successfully and efficiently, the coated mesh was first immersed in water at a temperature below LCST (it was 20 °C in this study) before being fixed in the separation device. This allows exposure of the hydrophilic PNIPAAm segments out of the surface, and thus the coated mesh is saturated with water, forming a stable barrier layer that prevents oil permeation. One can clearly observe that water (100 mL) flows through the separation unit only by gravity, while *n*-hexane (100 mL, dyed by ferrocene) is withheld above the mesh from Figure 6A. At the present state, the separation device plays a "water-removing" role. Conversely, the separation device can transform into an "oil-removing" one simply by switching the wettability of the coated mesh from the hydrophilic state to the hydrophobic state (a hair dryer was used in this work). At an elevated temperature, the temperature-sensitive PNIPAAm chains become collapsed and cooperate with perfluoroalkyl chains to form a stable hydrophobic and superoleophilic surface. As illustrated in Figure 6B, *n*-hexane is filtered easily into the flask and water is repelled. Both of the separation processes are vividly recorded by videos, which can be found in Video I and Video II in the Supporting Information.

According to the information (liquid volume and filtering time) recorded in the video, the penetration flux of water and *n*-hexane during separation are about 2.50 and 2.78 L s^{-1} m^{-2}. Compared to other advanced separation films based on polymeric materials, the present result shows its own advantages on water flux due to the hydrophilicity and good water retention capacity of the as-prepared mesh. For example, the flux for water using a poly(diallyldimethylammonium chloride)/sodium perfluorooctanoate/silica nanoparticle-based nanocomposite membrane is 0.48 L s^{-1} m^{-2},[63] and that using a mineral-coated polypropylene microfiltration membrane is 0.56 L s^{-1} m^{-2}.[64] As for the flux for oil, the value measured in this work is also higher than that obtained in a similar hexane/water separation system based on a SiO_2/carbon composite nanofibrous membrane (0.74 L s^{-1} m^{-2})[65] and a SiO_2 nanoparticle-doped polysulfone electrospun nanofiber membrane (2.16 L s^{-1} m^{-2}).[66] A schematic illustration of the microscopic water and oil wetting states at different temperatures is depicted in Figure 6C. A water-based barrier forms on the surface at a temperature below LCST, permitting water to go through the coated mesh quickly, whereas repelling oil. In the case of an "oil-removing" state, oil spreads rapidly on the as-fabricated mesh because of the chemical composition and surface-roughness-induced superoleophilicity, while water cannot penetrate through the film. Therefore, the water/oil mixture is separated with high flux and efficiency.

In addition to the water/*n*-hexane-layered system, other layered systems, such as water/*n*-heptane, water/*n*-octane, water/petroleum ether (60−90 °C), and water/diethyl ether, were investigated. All of the mixtures were separated efficiently with similar manners only by gravity. In all cases, oil liquid passes through the coated mesh more quickly than water because of the superoleophilicity of the rough mesh structure. The efficiency of separation processes for different organic solvent/water mixtures summarized in Figure 7 is determined by comparing the weight of water or oil before and after separation. 100% efficiency means the complete separation of water or organic solvent from the mixture. All of the separation processes have well efficiency of over 98%, which is comparable

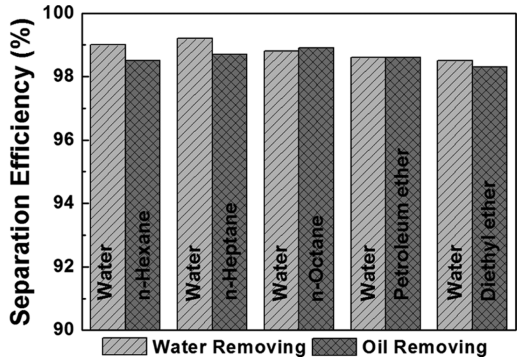

Figure 7. Separation efficiency of the coated mesh for different organic solvent/water mixtures (200 mL of a layered mixture in a volume ratio of 1:1 was used).

to or even higher than those of other advanced separation systems.[63−66]

During our experiments, five sets of organic solvent/water mixtures were separated by using the same as-fabricated mesh, and each separation process was repeated at last five times. After that, the morphology of the film remains well (Figure S3 in the Supporting Information), which indicates that the stability of the film is good in a certain period. These results indicate that the coated mesh with controllable wettability is very efficient and promising for application in water/oil separation.

4. CONCLUSION

In summary, a well-defined fluorinated thermosensitive block copolymer (PHFBMA-*b*-PNIPAAm) was synthesized through photoATRP. Kinetics study showed that photoATRP is a facile technique for the synthesis of polymer with high fidelity using a ppm-level high-oxidation-state transition-metal catalyst. The temporal control protocol applied during polymerization through intermittent on-and-off light conditions did not affect the polymer properties.

Subsequently, the as-prepared copolymer was used to fabricate a thermal-responsive surface with reversibly tunable wettability, which is attributed to the synergistic effect of the surface chemical composition, reorientation of the functional groups, and roughness in response to the temperature below and above the LCST.

On the basis of mechanism understanding, a smart separation device was constructed using a coated stainless steel mesh, which was prepared by copolymer solution casting. Such a smart device realized the on-demand separation of water/oil mixtures through adjustment of the temperature. The coated mesh acted as a "water-removing" separation unit at a temperature below LCST with a penetration flux of about 2.50 L s^{-1} m^{-2} and as an "oil-removing" device at a temperature above LCST with a penetration flux of about 2.78 L s^{-1} m^{-2}. Both of the separation processes ("water-removing" or "oil-removing") for different water/oil mixtures had a good separation efficiency above 98%. As a whole, the smart separation device has a promising perspective in the field of oily water preliminary treatment.

■ ASSOCIATED CONTENT

Supporting Information

The Supporting Information is available free of charge on the ACS Publications website at DOI: 10.1021/acs.iecr.5b02394.

DOI: 10.1021/acs.iecr.5b02394
Ind. Eng. Chem. Res. XXXX, XXX, XXX−XXX

Kinetics study, thermal property analysis, and morphology of the film used after numerous separation processes (PDF)
Video of a separation process (AVI)
Video of a separation process (AVI)

AUTHOR INFORMATION

Corresponding Author

*E-mail: luozh@sjtu.edu.cn. Tel.: +86-21-54745602. Fax: +86-21-54745602.

Notes

The authors declare no competing financial interest.

ACKNOWLEDGMENTS

The authors thank the National Natural Science Foundation of China (Grants 21276213 and U1462101) and the National High Technology Research and Development Program of China (Grant 2013AA032302) for supporting this work. The authors also thank the Center for Advanced Electronics Materials and Devices.

REFERENCES

(1) Yang, W. J.; Neoh, K.-G.; Kang, E.-T.; Teo, S. L.-M.; Rittschof, D. Polymer Brush Coatings for Combating Marine Biofouling. *Prog. Polym. Sci.* **2014**, *39*, 1017−1042.

(2) Liu, K.; Tian, Y.; Jiang, L. Bio-Inspired Superoleophobic and Smart Materials: Design, Fabrication, and Application. *Prog. Mater. Sci.* **2013**, *58*, 503−564.

(3) Ganesh, V. A.; Raut, H. K.; Nair, A. S.; Ramakrishna, S. A Review on Self-Cleaning Coatings. *J. Mater. Chem.* **2011**, *21*, 16304−16322.

(4) Anastasiadis, S. H. Development of Functional Polymer Surfaces with Controlled Wettability. *Langmuir* **2013**, *29*, 9277−9290.

(5) Ameduri, B. From Vinylidene Fluoride (VDF) to the Applications of VDF-Containing Polymers and Copolymers: Recent Developments and Future Trends. *Chem. Rev.* **2009**, *109*, 6632−6686.

(6) Boschet, F.; Ameduri, B. Co) polymers of Chlorotrifluoroethylene: Synthesis, Properties, and Applications. *Chem. Rev.* **2014**, *114*, 927−980.

(7) Yu, H.-J.; Luo, Z.-H. Novel Superhydrophobic Silica/poly(siloxane-fluoroacrylate) Hybrid Nanoparticles Prepared via Two-step Surface-initiated ATRP: Synthesis, Characterization, and Wettability. *J. Polym. Sci., Part A: Polym. Chem.* **2010**, *48*, 5570−5580.

(8) Yamaguchi, H.; Kikuchi, M.; Kobayashi, M.; Ogawa, H.; Masunaga, H.; Sakata, O.; Takahara, A. Influence of Molecular Weight Dispersity of Poly{2-(perfluorooctyl) ethyl acrylate} Brushes on Their Molecular Aggregation States and Wetting Behavior. *Macromolecules* **2012**, *45*, 1509−1516.

(9) van Zoelen, W.; Zuckermann, R. N.; Segalman, R. A. Tunable Surface Properties from Sequence-Specific Polypeptoid-Polystyrene Block Copolymer Thin Films. *Macromolecules* **2012**, *45*, 7072−7082.

(10) Guo, Y.; Tang, D.; Gong, Z. Superhydrophobic Films Fabricated by Electrospraying Poly(methyl methacrylate)-b-poly(dodecafluoroheptyl methacrylate) Diblock Copolymers. *J. Phys. Chem. C* **2012**, *116*, 26284−26294.

(11) Zhou, Y.-N.; Luo, Z.-H.; Chen, J.-H. Theoretical Modeling Coupled with Experimental Study on the Preparation and Characterization Comparison of Fluorinated Copolymers: Effect of Chain Structure on Copolymer Properties. *AIChE J.* **2013**, *59*, 3019−3033.

(12) Zhang, Q.; Wang, Q.; Zhan, X.; Chen, F. Synthesis and Performance of Novel Fluorinated Acrylate Polymers: Preparation and Reactivity of Short Perfluoroalkyl Group Containing Monomers. *Ind. Eng. Chem. Res.* **2014**, *53*, 8026−8034.

(13) Wadekar, M. N.; Patil, Y. R.; Ameduri, B. Superior Thermostability and Hydrophobicity of Poly(vinylidene fluoride-co-fluoroalkyl 2-trifluoromethacrylate). *Macromolecules* **2014**, *47*, 13−25.

(14) van Zoelen, W.; Buss, H. G.; Ellebracht, N. C.; Lynd, N. A.; Fischer, D. A.; Finlay, J.; Hill, S.; Callow, M. E.; Callow, J. A.; Kramer, E. J.; Zuckermann, R. N.; Segalman, R. A. Sequence of Hydrophobic and Hydrophilic Residues in Amphiphilic Polymer Coatings Affects Surface Structure and Marine Antifouling/Fouling Release Properties. *ACS Macro Lett.* **2014**, *3*, 364−368.

(15) Xia, F.; Zhu, Y.; Feng, L.; Jiang, L. Smart Responsive Surfaces Switching Reversibly between Super-hydrophobicity and Super-hydrophilicity. *Soft Matter* **2009**, *5*, 275−281.

(16) Xin, B. W.; Hao, J. C. Reversibly Switchable Wettability. *Chem. Soc. Rev.* **2010**, *39*, 769−782.

(17) Rios, F.; Smirnov, S. N. pH Valve Based on Hydrophobicity Switching. *Chem. Mater.* **2011**, *23*, 3601−3605.

(18) Smirnov, S. N.; Vlassiouk, I. V.; Lavrik, N. V. Voltage-Gated Hydrophobic Nanopores. *ACS Nano* **2011**, *5*, 7453−7461.

(19) Zhang, H.; Hou, X.; Zeng, L.; Yang, F.; Li, L.; Yan, D.; Tian, Y.; Jiang, L. Bioinspired Artificial Single Ion Pump. *J. Am. Chem. Soc.* **2013**, *135*, 16102−16110.

(20) Chen, L.; Wang, W.; Su, B.; Wen, Y.; Li, C.; Zhou, Y.; Li, M.; Shi, X.; Du, H.; Song, Y.; Jiang, L. A Light-Responsive Release Platform by Controlling the Wetting Behavior of Hydrophobic Surface. *ACS Nano* **2014**, *8*, 744−751.

(21) Zhang, L.; Zhang, Z.; Wang, P. Smart Surfaces with Switchable Superoleophilicity and Superoleophobicity in Aqueous Media: Toward Controllable Oil/Water Separation. *NPG Asia Mater.* **2012**, *4*, e8.

(22) Zhu, H.; Chen, D.; Li, N.; Xu, Q.; Li, H.; He, J.; Lu, J. Graphene Foam with Switchable Oil Wettability for Oil and Organic Solvents Recovery. *Adv. Funct. Mater.* **2015**, *25*, 597−605.

(23) Kwon, G.; Kota, A. K.; Li, Y. X.; Sohani, A.; Mabry, J. M.; Tuteja, A. On-Demand Separation of Oil-Water Mixtures. *Adv. Mater.* **2012**, *24*, 3666−3671.

(24) Cao, Y.; Liu, N.; Fu, C.; Li, K.; Tao, L.; Feng, L.; Wei, Y. Thermo and pH Dual-Responsive Materials for Controllable Oil/Water Separation. *ACS Appl. Mater. Interfaces* **2014**, *6*, 2026−2030.

(25) Xue, Z.; Cao, Y.; Liu, N.; Feng, L.; Jiang, L. Special Wettable Materials for Oil/Water Separation. *J. Mater. Chem. A* **2014**, *2*, 2445−2460.

(26) Wang, B.; Liang, W.; Guo, Z.; Liu, W. Biomimetic Super-lyophobic and Super-lyophilic Materials Applied for Oil/Water Separation: A New Strategy Beyond Nature. *Chem. Soc. Rev.* **2015**, *44*, 336−361.

(27) Chu, Z.; Feng, Y.; Seeger, S. Oil/Water Separation with Selective Superantiwetting/Superwetting Surface Materials. *Angew. Chem., Int. Ed.* **2015**, *54*, 2328−2338.

(28) Yu, X.; Wang, Z.; Jiang, Y.; Shi, F.; Zhang, X. Reversible pH-Responsive Surface: From Superhydrophobicity to Superhydrophilicity. *Adv. Mater.* **2005**, *17*, 1289−1293.

(29) Stratakis, E.; Mateescu, A.; Barberoglou, M.; Vamvakaki, M.; Fotakis, C.; Anastasiadis, S. H. From Superhydrophobicity and Water Repellency to Superhydrophilicity: Smart Polymer-Functionalized Surfaces. *Chem. Commun.* **2010**, *46*, 4136−4138.

(30) Sun, W.; Zhou, S.; You, B.; Wu, L. Polymer Brush-Functionalized Surfaces with Reversible, Precisely Controllable Two-Way Responsive Wettability. *Macromolecules* **2013**, *46*, 7018−7026.

(31) Cheng, M.; Liu, Q.; Ju, G.; Zhang, Y.; Jiang, L.; Shi, F. Bell-Shaped Superhydrophilic-Superhydrophobic-Superhydrophilic Double Transformation on a pH Responsive Smart Surface. *Adv. Mater.* **2014**, *26*, 306−310.

(32) Krupenkin, T. N.; Taylor, J. A.; Wang, E. N.; Kolodner, P.; Hodes, M.; Salamon, T. R. Reversible Wetting-Dewetting Transitions on Electrically Tunable Superhydrophobic Nanostructured Surfaces. *Langmuir* **2007**, *23*, 9128−9133.

(33) Pei, Y.; Travas-Sejdic, J.; Williams, D. E. Reversible Electrochemical Switching of Polymer Brushes Grafted onto Conducting Polymer Films. *Langmuir* **2012**, *28*, 8072−8083.

(34) Dos Ramos, L.; de Beer, S.; Hempenius, M. A.; Vancso, G. J. Redox-Induced Backbiting of Surface-Tethered Alkylsulfonate Amphiphiles: Reversible Switching of Surface Wettability and Adherence. *Langmuir* **2015**, *31*, 6343−6350.

DOI: 10.1021/acs.iecr.5b02394
Ind. Eng. Chem. Res. XXXX, XXX, XXX−XXX

(35) Groten, J.; Bunte, C.; Rühe, J. Light-Induced Switching of Surfaces at Wetting Transitions through Photoisomerization of Polymer Monolayers. *Langmuir* **2012**, *28*, 15038−15046.
(36) Abrakhi, S.; Péralta, S.; Fichet, O.; Teyssié, D.; Cantin, S. Poly (azobenzene acrylate-co-fluorinated acrylate) Spin-Coated Films: Influence of the Composition on the Photo-Controlled Wettability. *Langmuir* **2013**, *29*, 9499−9509.
(37) Zhou, Y.-N.; Li, J.-J.; Zhang, Q.; Luo, Z.-H. Light-Responsive Smart Surface with Controllable Wettability and Excellent Stability. *Langmuir* **2014**, *30*, 12236−12242.
(38) Zhou, Y.-N.; Li, J.-J.; Zhang, Q.; Luo, Z.-H. A Novel Fluorinated Polymeric Product for Photoreversibly Switchable Hydrophobic Surface. *AIChE J.* **2014**, *60*, 4211−4221.
(39) Yuan, W.; Jiang, G.; Wang, J.; Wang, G.; Song, Y.; Jiang, L. Temperature/Light Dual-Responsive Surface with Tunable Wettability Created by Modification with an Azobenzene-Containing Copolymer. *Macromolecules* **2006**, *39*, 1300−1303.
(40) Liu, X. J.; Ye, Q.; Yu, B.; Liang, Y. M.; Liu, W. M.; Zhou, F. Switching Water Droplet Adhesion Using Responsive Polymer Brushes. *Langmuir* **2010**, *26*, 12377−12382.
(41) Li, J.-J.; Zhou, Y.-N.; Luo, Z.-H. Thermo-responsive Brush Copolymers with Structure-Tunable LCST and Switchable Surface Wettability. *Polymer* **2014**, *55*, 6552−6560.
(42) Li, J.-J.; Zhou, Y.-N.; Luo, Z.-H. Thermal-Responsive Block Copolymers for Surface with Reversible Switchable Wettability. *Ind. Eng. Chem. Res.* **2014**, *53*, 18112−18120.
(43) Xue, B.; Gao, L.; Hou, Y.; Liu, Z.; Jiang, L. Temperature Controlled Water/Oil Wettability of a Surface Fabricated by a Block Copolymer: Application as a Dual Water/Oil on-off Switch. *Adv. Mater.* **2013**, *25*, 273−277.
(44) Jiang, B.; Zhang, L.; Liao, B.; Pang, H. Self-assembly of Well-defined Thermo-responsive Fluoropolymer and Its Application in Tunable Wettability Surface. *Polymer* **2014**, *55*, 5350−5357.
(45) Ganesh, V. A.; Ranganath, A. S.; Sridhar, R.; Raut, H. K.; Jayaraman, S.; Sahay, R.; Ramakrishna, S.; Baji, A. Cellulose Acetate-Poly(N-isopropylacrylamide)- Based Functional Surfaces with Temperature-Triggered Switchable Wettability. *Macromol. Rapid Commun.* **2015**, *36*, 1368−1373.
(46) Schild, H. G. Poly(N-isopropylacrylamide): Experiment, Theory and Application. *Prog. Polym. Sci.* **1992**, *17*, 163−249.
(47) Sun, T.; Wang, G.; Feng, L.; Liu, B.; Ma, Y.; Jiang, L.; Zhu, D. Reversible Switching Between Superhydrophilicity and Superhydrophobicity. *Angew. Chem., Int. Ed.* **2004**, *43*, 357−360.
(48) Chen, L.; Liu, M.; Lin, L.; Zhang, T.; Ma, J.; Song, Y.; Jiang, L. Thermal-responsive Hydrogel Surface: Tunable Wettability and Adhesion to Oil at The Water/Solid Interface. *Soft Matter* **2010**, *6*, 2708−2712.
(49) Ameduri, B. Controlled Radical (Co)polymerization of Fluoromonomers. *Macromolecules* **2010**, *43*, 10163−10184.
(50) Matyjaszewski, K.; Tsarevsky, N. V. Macromolecular Engineering by Atom Transfer Radical Polymerization. *J. Am. Chem. Soc.* **2014**, *136*, 6513−6533.
(51) Matyjaszewski, K.; Jakubowski, W.; Min, K.; Tang, W.; Huang, J.; Braunecker, W. A.; Tsarevsky, N. V. Diminishing Catalyst Concentration in Atom Transfer Radical Polymerization with Reducing Agents. *Proc. Natl. Acad. Sci. U. S. A.* **2006**, *103*, 15309−15314.
(52) Magenau, A. J. D.; Strandwitz, N. C.; Gennaro, A.; Matyjaszewski, K. Electrochemically Mediated Atom Transfer Radical Polymerization. *Science* **2011**, *332*, 81−84.
(53) Konkolewicz, D.; Wang, Y.; Zhong, M.; Krys, P.; Isse, A. A.; Gennaro, A.; Matyjaszewski, K. Reversible-Deactivation Radical Polymerization in the Presence of Metallic Copper. A Critical Assessment of the SARA ATRP and SET-LRP Mechanisms. *Macromolecules* **2013**, *46*, 8749−8772.
(54) Zhou, Y.-N.; Luo, Z.-H. Copper(0)-Mediated Reversible-Deactivation Radical Polymerization: Kinetics Insight and Experimental Study. *Macromolecules* **2014**, *47*, 6218−6229.
(55) Poelma, J. E.; Fors, B. P.; Meyers, G. F.; Kramer, J. W.; Hawker, C. J. Fabrication of Complex Three-Dimensional Polymer Brush Nanostructures through Light-Mediated Living Radical Polymerization. *Angew. Chem., Int. Ed.* **2013**, *52*, 6844−6848.
(56) Yan, J.; Li, B.; Zhou, F.; Liu, W. Ultraviolet Light-Induced Surface-Initiated Atom-Transfer Radical Polymerization. *ACS Macro Lett.* **2013**, *2*, 592−596.
(57) Zhang, T.; Chen, T.; Amin, I.; Jordan, R. ATRP with A Light Switch: Photoinduced ATRP Using a Household Fluorescent Lamp. *Polym. Chem.* **2014**, *5*, 4790−4796.
(58) Anastasaki, A.; Nikolaou, V.; Zhang, Q.; Burns, J.; Samanta, S. R.; Waldron, C.; Haddleton, A. J.; McHale, R.; Fox, D.; Percec, V.; Wilson, P.; Haddleton, D. M. Copper(II)/Tertiary Amine Synergy in Photoinduced Living Radical Polymerization: Accelerated Synthesis of ω-Functional and α,ω-Heterofunctional Poly(acrylates). *J. Am. Chem. Soc.* **2014**, *136*, 1141−1149.
(59) Ribelli, T. G.; Konkolewicz, D.; Bernhard, S.; Matyjaszewski, K. How Are Radicals (Re)Generated in Photochemical ATRP? *J. Am. Chem. Soc.* **2014**, *136*, 13303−13312.
(60) Anastasaki, A.; Nikolaou, V.; McCaul, N. W.; Simula, A.; Godfrey, J.; Waldron, C.; Wilson, P.; Kempe, K.; Haddleton, D. M. Photoinduced Synthesis of α,ω-Telechelic Sequence-Controlled Multiblock Copolymers. *Macromolecules* **2015**, *48*, 1404−1411.
(61) Honda, K.; Morita, M.; Otsuka, H.; Takahara, A. Molecular Aggregation Structure and Surface Properties of Poly(fluoroalkyl acrylate) Thin Films. *Macromolecules* **2005**, *38*, 5699−5705.
(62) Zhou, Y.-N.; Luo, Z.-H. An Old Kinetic Method for A New Polymerization Mechanism: Toward Photochemically Mediated ATRP. *AIChE J.* **2015**, *61*, 1947−1958.
(63) Yoon, H.; Na, S.-H.; Choi, J.-Y.; Latthe, S. S.; Swihart, M. T.; Al-Deyab, S. S.; Yoon, S. S. Gravity-Driven Hybrid Membrane for Oleophobic−Superhydrophilic Oil−Water Separation and Water Purification by Graphene. *Langmuir* **2014**, *30*, 11761−11769.
(64) Chen, P. C.; Xu, Z. K. Mineral-coated Polymer Membranes with Superhydrophilicity and Underwater Superoleophobicity for Effective Oil/Water Separation. *Sci. Rep.* **2013**, *3*, 2776.
(65) Tai, M. H.; Gao, P.; Tan, B. Y. L.; Sun, D. D.; Leckie, J. O. Highly Efficient and Flexible Electrospun Carbon−Silica Nanofibrous Membrane for Ultrafast Gravity-Driven Oil-Water Separation. *ACS Appl. Mater. Interfaces* **2014**, *6*, 9393−9401.
(66) Obaid, M.; Tolba, G. M. K.; Motlak, M.; Fadali, O. A.; Khalil, K. A.; Almajid, A. A.; Kim, B.; Barakat, N. A. M. Effective Polysulfone-Amorphous SiO_2 NPs Electrospun Nanofiber Membrane for High Flux Oil/Water Separation. *Chem. Eng. J.* **2015**, *279*, 631−638.

DOI: 10.1021/acs.iecr.5b02394
Ind. Eng. Chem. Res. XXXX, XXX, XXX−XXX